J Sol-Gel Sci Technol (2013) 65:195–203
DOI 10.1007/s10971-012-2924-2

ORIGINAL PAPER

# Enhanced photo-catalytic activity of $TiO_2$ nanostructured thin films under solar light by Sn and Nb co-doping

**Behzad Koozegar Kaleji · Navid Hosseinabadi · Akira Fujishima**

Received: 16 August 2012 / Accepted: 16 November 2012 / Published online: 27 November 2012


**Abstract** In this study, preparation of Sn and Nb co-doped $TiO_2$ dip-coated thin films on glazed porcelain substrates via sol–gel process have been investigated. The effects of co-doping content on the structural, optical, and photo-catalytic properties of applied thin films have been studied by X-ray diffraction (XRD), field emission SEM (FE-SEM), high resolution transmission electron microscopy (HR-TEM), and UV–Vis absorption spectroscopy. Surface chemical state of thin films was examined by atomic X-ray photoelectron spectroscopy (XPS). XRD results suggest that adding impurities has a great effect on the crystallinity and particle size of $TiO_2$. Titania Rutile phase formation in thin film was promoted by $Sn^{4+}$ addition but was inhibited by $Nb^{5+}$ doping. The prepared co-doped $TiO_2$ photo-catalyst films showed optical absorption edge in the visible light area and exhibited excellent photo-catalytic ability for degradation of methylene blue (MB) solution under solar irradiation. Comparison with undoped and Sn or Nb-doped $TiO_2$, codoped $TiO_2$ shows an obviously higher catalytic activity under solar irradiation.

B. K. Kaleji (✉)
Department of Materials Engineering, Faculty of Engineering, Malayer University, P.O.Box 65719-95863, Malayer, Iran
e-mail: bkaleji@yahoo.com; b.kaleji@malayeru.ac.ir

N. Hosseinabadi
Department of Materials Engineering, Faculty of Engineering, Tarbiat Modares University, P.O.Box 14115-143, Tehran, Iran

A. Fujishima
Photo-catalystic Group, Kanagawa Academy of Science and Technology, kanagawa, Japan

A. Fujishima
Tokyo University of Science, 1-3 Kagurazaka, Shinjuku-ku, Tokyo 162-8601, Japan

**Keywords** Titania thin film · Sol–gel dip coating · Co-dopant · Photo-catalytic activity · Optical properties

## 1 Introduction

Titanium oxide is a well-known photocatalyst working in the ultraviolet (UV) region of light with a band gap of 3.2 eV. Numerous reports are available regarding the shifting of wavelength corresponding to the onset of absorption from UV to visible region of light in $TiO_2$ as a consequence of doping with cationic or anionic dopants. Anionic dopants such as nitrogen, sulphur, carbon, and fluorine lead to narrowing of the band gap of $TiO_2$ which results in visible light absorption and improved photo-catalytic activity [1–3]. Doping $TiO_2$ with antimony and chromium results in the shifting of absorption band from UV to visible light region and exhibits photo-catalytic activity for $O_2$ generation from aqueous silver nitrate solution under visible light irradiation [4]. $TiO_2$ doped with Ce, V, Cu, Sn, Nd, Fe, Cr, or Co shows a red shift in the absorption band compared to pure $TiO_2$, and considerable photo-catalytic activity under visible light irradiation [5–11]. Doping with lanthanide ions such as $Eu^{3+}$, $Pr^{3+}$ and $Yb^{3+}$ in $TiO_2$ was found to improve the photo-catalytic activity for the photo degradation of salicylic acid and t-cinnamic acid [12]. The enhanced degradation was attributed to the formation of Lewis acid–base complex between the lanthanide ions and the reactants at the photocatalyst interface. The photo-excited wavelength of the $TiO_2$–$SnO_2$ prepared by ball milling shows a red shift of 20 nm in its absorption spectrum and increase in the photo-catalytic activity for the degradation of monocrotophos compared to pure $TiO_2$ [13]. The increased photo-catalytic activity was explained on the basis of the photo generated

charge separation efficiency of the coupled $TiO_2$–$SnO_2$. Sensitization of Cu doped $TiO_2$ with eosin improved the photo-catalytic activity for water splitting under visible light irradiation [7]. Doping $TiO_2$ with 0.1 % Nd and impregnation with Pt produced enhanced photo-catalytic activity for water splitting due to the prevention of phase transformation of $TiO_2$ from anatase to rutile and inhibition of particle growth [14]. Some recent studies have revealed that the oxygen deficient sites play a crucial role in the visible light induced photo-catalytic activity of $TiO_2$. Ihara et al. [15] have reported that the low temperature $H_2$ plasma treated $TiO_2$ and nitrogen doped $TiO_2$ [16] show visible light photo-catalytic activity due to the presence of oxygen deficient sites. Visible light absorption of $TiO_2$, reduced in different polymeric media, originates from colour centers (defects associated with oxygen vacancies) rather than due to a narrowing of the original band gap of $TiO_2$ [17]. Prokes et al. [18] have proposed that the visible light absorption of titanium oxynitride is due to the oxygen hole centre created during the surface modification process by nitrogen near the surface of the nano colloid. The visible light photo-catalytic activity observed due to the oxygen vacancies in $TiO_2$ is found to decrease after an optimum value [19].

Among the advantages of titania as a photocatalyst, its excellent (photo) chemical stability, low cost, and non-toxicity can be cited. However, its wide band-gap energy (ca. 3.0 eV for rutile and 3.2 eV for anatase) means that only 5 % of solar spectrum is used. Moreover, $TiO_2$ presents a relatively high electron–hole recombination rate which is detrimental to its photoactivity. In this sense, doping with metals or metal oxides could make a double effect:

1. It could reduce the band gap energy, thus shifting the absorption band to the visible region.
2. Metals could provoke a decrease in electron–hole recombination rate, acting as electron traps.

In our previous research we studied the effect of doping Sn (up to 30 mol%) and Nb (up to 20 mol%) on photo-catalytic behavior of titania based thin films. We found that 15 mol% of Sn and 1 mol% on Nb shows the most significant improvement on photo-catalytic behavior of $TiO_2$ under UV irradiation [20, 21]. In the present study, Sn and Nb have been selected as co dopnats to increase the photo-catalytic activity of thin films at the solar light wavelengths. The thin films were applied by sol–gel dip-coating process. The effect of the dopant cations on the structure and the phase stability was studied in a systematic way. The efficiency of these samples as photocatalysts for the degradation of MB, as organic compound model, under solar excitation, was investigated.

## 2 Experimental procedures

### 2.1 Preparation of the thin films

The preparation of precursor solution for Sn/Nb co-doped $TiO_2$ thin films is described as follows: $TiO_2$, $SnO_2$ and $Nb_2O_5$ sols were prepared, separately. For the preparation of $TiO_2$ sol, titanium (IV) butoxide (TBT = Ti $(OC_4H_9)_4$, Aldrich) was selected as titanium source. First, 0.35 mol ethanol (EtOH, Merck) and 0.04 mol ethyl acetoacetate (EAcAc is as a sol stabilizer during preparation of sol and also chelating agent during coating, Merck) were mixed, and then 0.01 mol TBT was added by the rate of 1 ml/min to the mixture at the ambient temperature (25 °C). The solution was continuously stirred for 45 min, followed by the dropping of $HNO_3$ as catalyst to the solution until pH of 3. De-ionized water was added to the solution slowly to initiate hydrolysis process. Solution was aged for 24 h in order to complete all reactions. The chemical composition of the resultant alkoxide solution was TBT:$H_2O$:$HNO_3$:EAcAc:EtOH = 1:10:1:4:35 in molar ratio. In order to prepare $SnO_2$·sol and $Nb_2O_5$·sol, stannous chloride ($SnCl_2{\cdot}2H_2O$, Merck) and Niobium chloride were dissolved in EtOH with molar ratio of $SnCl_2{\cdot}2H_2O$:EtOH = 1:35 and $NbCl_5$:EtOH = 2:35 at ambient temperature with continuous stirring. Solutions were aged for 24 h in order to complete all reactions. Then, mixtures of $TiO_2$, $SnO_2$, and $Nb_2O_5$ were made with different mol ratios of Sn and Nb (Ti-15 %Sn-1 %Nb) at the ambient temperature. The Sn/Nb co-doped thin films were applied on the glazed porcelain substrates with the prepared sol solutions by dipping-withdrawing at room temperature with withdrawal speed of 10 mm/min.

The porcelain substrate composition was $Al_2O_3$: 45.12, $SiO_2$: 43.83, BaO: 6.18, $K_2O$: 3.63, $Na_2O$: 0.58, MgO: 0.39, CaO: 0.27 wt%. Glazed composition contained $SiO_2$: 64.45, $Al_2O_3$: 16.56, CaO: 6.07, $K_2O$: 5.1 MgO: 4.36, $Fe_2O_3$: 3.46 wt%. Porcelain and glaze compositions were reported by substrate manufacturer with formal report.

Substrate dimensions were 30 × 15 × 1 mm. The substrates were degreased in ethanol and cleaned in de-ionized water for 15 min and acetone with supersonic wave. The treated substrate samples were dried at 80 °C for 1 h. In order to prevent diffusion of porcelain substrate and glaze elements to final thin film, one interlayer (buffer layer) $SiO_2$ thin film with withdrawal speed of 10 mm/min was applied. Silica sol contains tetra ethyl orthosilicate (TEOS, Merck): EtOH:$H_2O$:HCl with 1:3.8:1:0.01 molar ratios and calcined at 400 °C for 1 h. Samples were dried at 100 °C for 1 h after each coating cycle and finally heated at a rate of 2 °C/min and calcined at 475 °C for 1 h in air atmosphere.

Substrates were coated with one $SiO_2$ (buffer layer) and two Sn/Nb co-doped $TiO_2$ layers.

### 2.2 Characterization methods

Differential thermal analysis (DTA) and thermogravimetric (TG) were used in order to determine crystallization temperature with a heating rate of 10 °C/min (STA 1,460 equipment). XRD pattern and phase identification of thin films were recorded using X-ray diffraction analysis (Philips, MPD-XPERT, λ: $Cu_{k\alpha} = 0.154$ nm). The samples were scanned in the 2θ range of 20–70°. Morphology of the thin films was observed using scanning electron microscopy (SEM, XL30 Series) with an accelerating voltage of 10–15 kV. X-ray photoelectron spectroscopy (XPS) spectra were recorded by a PHI 5000C ESCA spectrometer using Mg Ka radiation ($h\upsilon = 1{,}253.6$ eV). The pressure of the analyzer chamber was maintained at $5 \times 10^{-8}$ Pa. Spectra were calibrated with respect to the C1s peak at 284.6 eV.

$N_2$ adsorption–desorption isotherms were determined in a surface analyzer equipment (BEL Japan Inc., Osaka, Japan) at 77 K. BET surface area and BJH analyses were used to determine the total specific surface area and the pore size distribution.

In order to make TEM foils, the films were removed from the substrates by water flotation. Droplets of the sol–gel material were also deposited on plain (un-coated) copper grids so as to form free-standing films for in situ hot-stage experiments in the TEM. Conventional TEM imaging and electron diffraction analysis was carried out using an EM-2100F-JEOL-Tokyo-Japan with acceleration voltage of 200 kV.

### 2.3 Photo-catalytic activity measurement

The photo-catalytic activity was evaluated by monitoring the degradation of MB solution (5 ppm) under UV and solar illumination. The samples were placed in 20 ml aqueous MB solution and were kept in dark for 2 h. They were then irradiated from top using a UV lamp (Philips 8 W, 360 nm) and solar irradiation (the total accumulated UV light (350–400 nm) and the total accumulated visible light (400–750 nm) were 6.786 and 78.834 kJ/L, respectively) using costume made apparatus. The intensity of the MB characteristic band at 660 nm (I660) in the obtained UV–vis spectrum (Varian cary 50 spectrophotometer) was used to determine the concentration of MB in the solution ($C_t$).

The degradation rate of MB, which represents the photo-catalytic efficiency of the films, can be determined by Eq. 1.

$$d(\%) = (C_0 - C_t)/C_0 \times 100 \quad (1)$$

Where d is degradation rate, $C_t$ is concentration after radiation and $C_0$ is concentration before radiation [22].

## 3 Results and discussion

Figure 1 shows the XRD patterns of the films without and with Sn, Nb dopant heat treated at 475 °C for 1 h. X-ray diffraction peak at 25.5° corresponds to characteristic peak of crystal plane (1 0 1) of anatase, at 27.6° corresponds to characteristic peak of crystal plane (1 1 0) of rutile in films. According to the XRD patterns, the pure $TiO_2$ (T) constituted of pure anatase phase.

All thin films were identified as the mixture polymorphs of anatase (JCPDS: No. 21-1272) and rutile (JCPDS: No.21-1276), without any impurity phase. In the phase composition, anatase appeared as the main phase, and rutile crystallization was promoted by $Sn^{4+}$ doping but was inhibited by $Nb^{5+}$ doping. With the addition of Sn 15 % and Nb 1 %, the intensity of the (101) diffraction peak became weaker than that of the pure $TiO_2$ film, suggesting that the film with Sn and Nb co-doping experienced lower crystallization. Other co-doped samples were also rutile $TiO_2$ and no signs of metal or oxide phases of Tin or Niobium were detected. This suggests the incorporation of $Sn^{4+}$ and $Nb^{5+}$ in $TiO_2$ lattice [23, 24].

The diffraction peaks of rutile crystallites appeared in X-ray profiles with increasing Sn dopant in thin films. The addition of Sn has a promoting effect on the transformation of anatase to rutile crystalline phase [25, 26], due to the rutile like structure of $SnO_2$-cassiterite phase. It is also found that the peak position of (1 0 1) anatase and (1 1 0) rutile planes shift to a smaller diffraction angle with increasing Sn content in $TiO_2$ thin films. This may results from the exchange of Ti with Sn in the $TiO_2$ lattice.

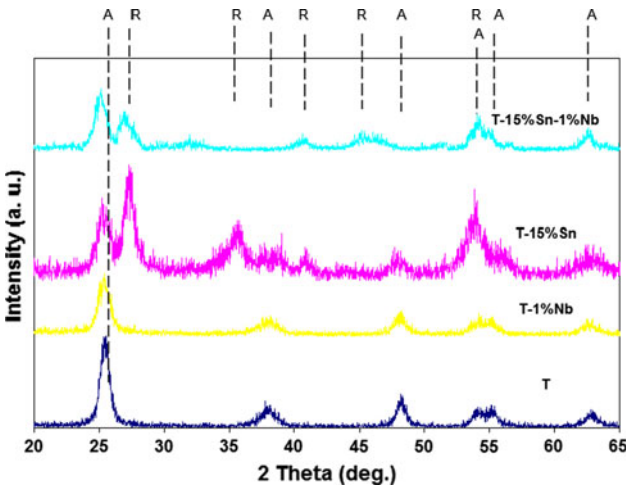


**Fig. 1** XRD spectra of the pure and doping $TiO_2$ films

**Table 1** The characteristic of dip-coated thin films after thermal treatment at 475 °C

| Sample | %A | %R | $d_A$ (nm) | $d_R$ (nm) | a = b (Å) | c (Å) | $V_{u.c}$ (Å$^3$) |
|---|---|---|---|---|---|---|---|
| T | 100 | – | 15.1 | – | 3.776 | 9.341 | 133.162 |
| T-1 %Nb | 100 | – | 12.2 | – | 3.786 | 9.347 | 133.972 |
| T-15 %Sn | 36.2 | 63.8 | 12.1 | 14.8 | 3.809 | 2.199 | 31.907 |
| T-15 %Sn-1 %Nb | 66.7 | 33.3 | 7.1 | 12.3 | 3.812 | 10.274 | 148.813 |

The average crystallite size of thin films (D) was determined from the XRD patterns, according to the Scherrer Eq. (2) [27]

$$D = k\lambda/\beta \cos\theta \tag{2}$$

where k is a constant (shape factor, about 0.9), λ the X-ray wavelength (0.154 nm), β the full width at half maximum (FWHM) of the diffraction peak, and θ is the diffraction angle. The values of β and θ of anatase and rutile phases were taken from anatase (1 0 1) and rutile (1 1 0) planes diffraction lines, respectively.

The amount of rutile in the samples was calculated using the following equation [28]

$$X_R = (1 + 0.8I_A/I_R)^{-1} \tag{3}$$

where $X_R$ is the mass fraction of rutile in the samples, and $I_A$ and $I_R$ are the X-ray integrated intensities of (101) reflection of the anatase and (110) reflection of rutile, respectively. The diffraction peaks of crystal planes (101) (200), and (105) of Anatase phase in XRD patterns were selected to determine the lattice parameters of the $TiO_2$ and doped $TiO_2$ thin films. The lattice parameters were obtained by using the Eq. (4) [27]

$$\begin{aligned} &(Bragg's\ law) : 2d_{(hkl)} \sin\theta = \lambda \\ &(1/d_{(hkl)})^2 = (h/a)^2 + (k/b)^2 + (l/c)^2 \end{aligned} \tag{4}$$

where $d_{(hkl)}$ is the distance between the crystal planes of (hkl); λ is the wavelength of X-ray used in the experiment; θ is the diffraction angle of the crystal plane (hkl); hkl is the crystal plane index; and *a, b*, and *c* are lattice parameters (in Anatase form, $a = b \neq c$).

The characteristic of all thin films after thermal treatment at 475 °C is reported at Table 1. By increasing Sn dopant, transformation of anatase to rutile phase was promoted, the amount of rutile phase structure was increased, and a decrease in the crystalline size was detected. The decrease in crystal size can be attributed to the presence of

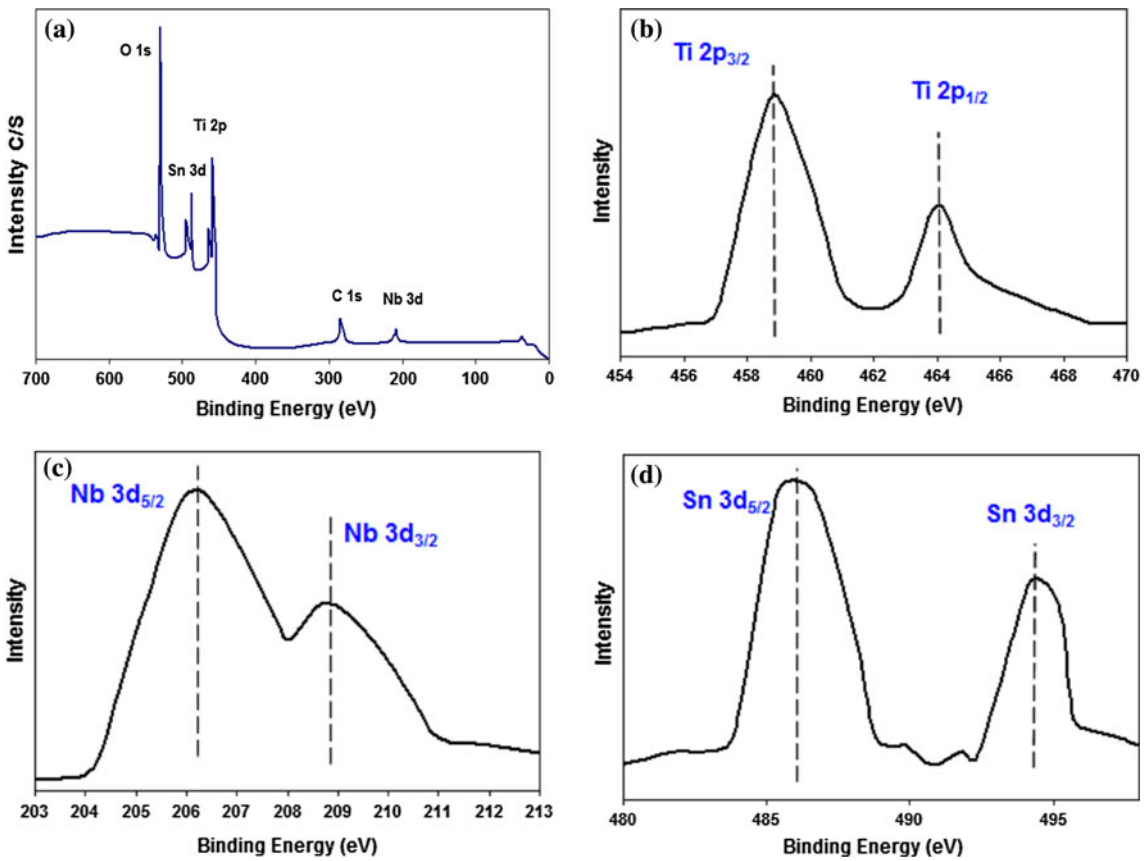


**Fig. 2** XPS analysis of calcined Sn/Nb co-doped $TiO_2$ thin film. **a** Survey analysis (Broad scan), **b** Ti 2p, **c** Sn 3d, **d** Nb 3d

Sn–O–Ti in the Sn-doped $TiO_2$ thin films which inhibits the growth of crystal grains [29].

Compared with those of pure $TiO_2$ films, for doped $TiO_2$ films, average anatase crystallite sizes decreased. It is found that the Nb dopants can inhibit the anatase grain growth. The $Nb^{5+}$ radius (0.70 Å) is slightly bigger than $Ti^{4+}$ radius (0.64 Å) and this means that $Nb^{5+}$ induces slight stress in $TiO_2$ lattice, which may hinder the growth of the $TiO_2$ crystallites as was found by Sharma and Bhatnagar [23].

Also, the lattice parameters and cell volume of the $TiO_2$ and doped $TiO_2$ thin films are summarized in Table 1.

It is obvious that the lattice parameters and cell volume of the doped $TiO_2$ thin films increase with increasing amount of Sn an Nb substitution for $Ti^{4+}$ in titania lattice.

XPS is a highly sensitive technique of surface analysis, and is an effective method to investigate the surface composition and chemical states of solid samples. XPS measurements were carried out to determine the surface composition and chemical state of Sn/Nb co-doped $TiO_2$ thin film calcined at 475 °C. The XPS survey spectrum in Fig. 2 demonstrates the presence of titanium, oxygen, carbon, tin, and Nb on the surface (Fig. 2a). All the binding energies were referenced to the adventitious C 1s peak at 284.6 eV.

The binding energy of Ti $2p_{3/2}$ and Ti $2p_{1/2}$ were observed at approximately 458.8 and 464.1 eV, respectively, indicating that the Ti element mainly existed as the chemical state of $Ti^{4+}$ [30]. XPS spectra of Sn 3d region are given in Fig. 2c. Two peaks corresponding to Sn $3d_{5/2}$ and Sn $3d_{3/2}$ are observed. The peak position corresponding to Sn $3d_{5/2}$ is located between those of Sn $3d_{5/2}$ in $SnO_2$ (486.5 eV) and Sn $3d_{5/2}$ in metallic Sn (485.0 eV), which is ascribed to incorporated $Sn^{4+}$ in the lattice of $TiO_2$ [31].

Figure 2d shows the Nb 3d spectrum for the doped film exhibiting two peaks at 206.3 and 208.8 eV [32]. The peaks represent the $3d_{5/2}$ and $3d_{3/2}$ components, respectively, with a spin–orbit splitting of 2.5 eV. The center of the Nb $3d_{3/2}$ peak corresponds to that of $Nb^{5+}$ oxidation state.

The nitrogen adsorption–desorption isotherm at 77 K and the BJH pore size distribution of sample calcined at 475 °C are showed in Fig. 3. It can be observed that the sample exhibits the classical shape of a type IV isotherm according to the IUPAC classification, typical for mesoporous solids [33]. The existence of the hysteresis loop in the isotherms is due to the capillary condensation of $N_2$ gas occurring in the mesopores. The surface area and the mean pore diameter of co-doped film calcined at 475 °C are 262.34 $m^2/g$ and 5.7 nm, respectively.

Table 2 shows the results from surface area measurements of the different samples. As can be seen, the co-doped $TiO_2$ film has larger surface area.

Figure 4 shows the UV–vis spectra of the pure $TiO_2$ and the doped $TiO_2$ thin films deposited on glazed porcelain substrates in the wavelength range of 250–600 nm. In this figure, the absorption edge of Sn-doped $TiO_2$ thin films shifts towards longer wavelengths, whereas absorption edge of Nb-doped $TiO_2$ thin films shifts towards shorter wavelengths. It indicates a decrease (Sn doping) or increase (Nb doping) in the energy band gap (inset in Fig. 4).

The energy band gap corresponds to the absorption limit and can be roughly evaluated by using following equation:

$$E_g = \frac{1240}{\lambda_{edge}}(eV) \quad (5)$$

where $\lambda_{edge}$ represents the absorption limit of the semiconductor. $\lambda_{edge}$ can be extracted from the absorption spectrum by carrying out the first derivative of absorbance with respect to wavelength near the absorption edge and finding the point at which the derivative spectrum reaches its minimum value. This point is actually the reflection

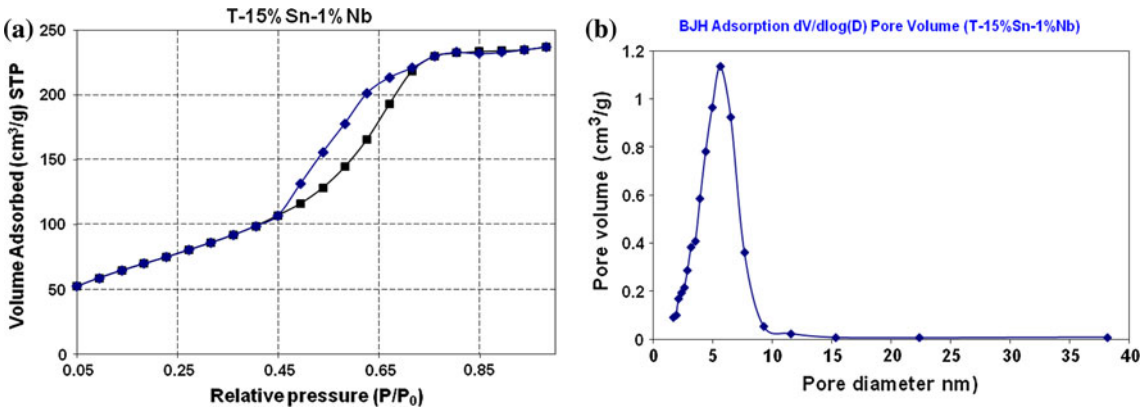


**Fig. 3** Nitrogen adsorption–desorption isotherm

**Table 2** Surface area measurement of the different samples

| Sample code | BET surface area ($m^2$/g) |
|---|---|
| T (undoped) | 85.93 |
| T-1 %Nb | 150.61 |
| T-15 %Sn | 106.97 |
| T-15 %Sn-1 %Nb | 262.34 |

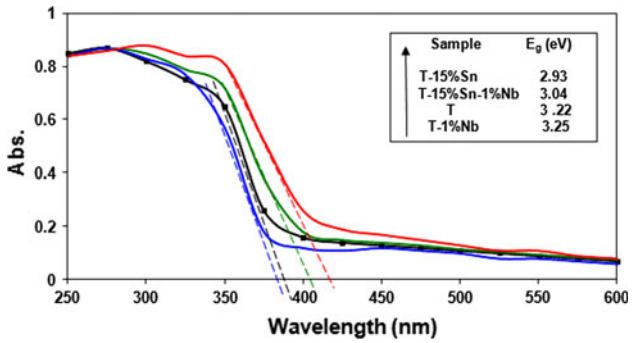


**Fig. 4** UV–vis absorption spectra of pure $TiO_2$ and doped thin films deposited on glazed porcelain substrate (calcined at 475 °C) with calculated energy band gaps of samples

point of the absorption curve. The tangent line of the absorption curve at the reflection point intersects with the x-axis on which absorbance reaches 0 and indicates $\lambda_{edge}$.

Doping $Sn^{4+}$ has been found to be located approaching and below the conduction band [8]. Therefore, the red shift of the absorption edge for the Sn-doped $TiO_2$ should be the result of the electronic transition from the valance band to the doping energy level. On the other hand, according to the XRD results, doping with Sn had accelerated the transformation from anatase to rutile phase of $TiO_2$, and the rutile phase has a band gap smaller than that of anatase, so this transformation should be another reason for the red shift.

The band gap of the pure $TiO_2$ thin film was about 3.22 eV and had increased to 3.25 eV with increasing Nb content. The widening of the band gap can be explained by the Burstein-Moss (BM) effect [34], in which the lowest states in the conduction band were blocked, and transitions can take place only to energies higher than Fermi energy. Thus, the band gap became widened with increasing Nb content. The observed values were higher than the band gap of both bulk and thin film $TiO_2$ in the anatase phase. The reported values were 3.18 eV [35] for bulk material and in the range 3.2–3.23 eV for thin films [36].

The absorption spectrum of co-doped $TiO_2$ shows that co-doping not only leads to a red-shift of absorption edge but also significantly enhances the absorption of visible light. The absorption of Sn/Nb co-doping samples in visible region is much higher than those of single doped samples (Nb-doped $TiO_2$) and lesser than Sn-doped $TiO_2$.

Figure 5 shows the normalized concentration at 660 nm absorption of the MB solutions separated from the $TiO_2$ thin film as a photocatalyst under various time irradiations (0–120 min) to determine the photo-catalytic degradation: a under the UV irradiation and b under the visible light irradiation.

According to Figure 5a, the order of photo-catalytic activity of $TiO_2$ thin films at 120 min under the UV irradiation was as following: T-15 %Sn-1 %Nb > T-1 %Nb > T-15 %Sn >T, but under the sun light irradiation (Fig. 5b), was T-15 % Sn-1 %Nb > T-15 %Sn > T-1 %Nb > T which suggests that the doping enhances the photo-catalytic activity of $TiO_2$ under both conditions. Non-doped Titania has lowest response in all irradiation ranges. T coatings have better response under UV light because of $E_g$ around 3.22 eV. This energy band is in UV light range. Near 90.4 % of MB was decomposed in the presence of T-15 %Sn-1 %Nb film after UV irradiation for 120 min, while the values in the presence of T-1 %Nb, T-15 %Sn and T film are 76.2, 42.4 and 36.4 %, respectively. Also, photo-catalytic activity of $TiO_2$ thin films at 120 min under the sun light

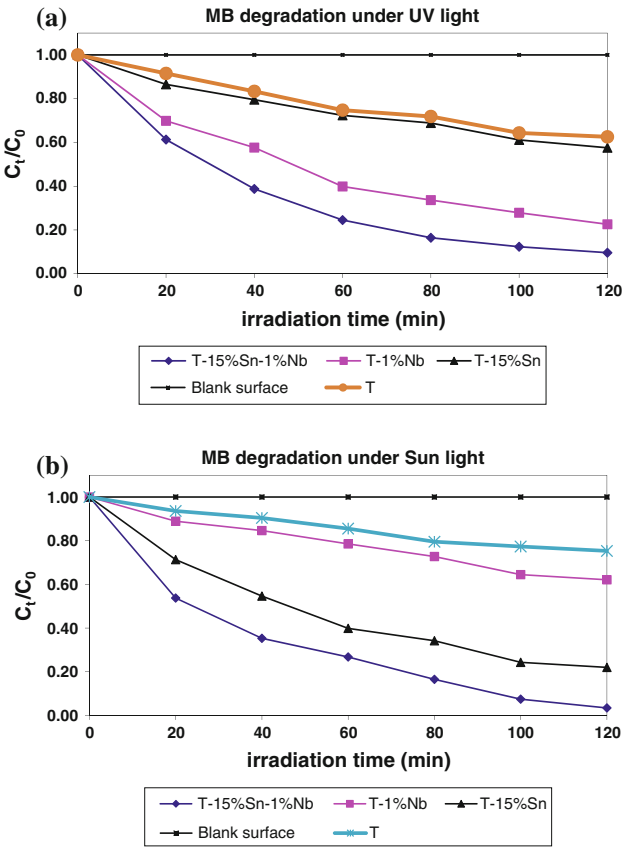


**Fig. 5** Normalized concentration at 660 nm absorption of the MB solutions under various time irradiations, **a** under the UV irradiation and **b** under the sun light irradiation

irradiation obtained 96.5, 78.1, 37.8 and 24.7 % in the presence of T-15 %Sn-1 %Nb, T-15 %Sn, T-1 %Nb and T thin film, respectively.

Some studies indicated that the photo-catalytic activity of $TiO_2$ catalysts depends strongly on two factors: adsorption behavior and the separation efficiency of electron–hole pairs [37, 38]. On the one hand, the BET results showed that the specific surface areas of the catalysts increased from 85.93 $m^2/g$ for undoped $TiO_2$ to 262.34 $m^2/g$ for co-doped $TiO_2$, significantly (shown in Table 2). The larger specific surface area of co-doped $TiO_2$ catalysts would be beneficial to achieve better adsorption of MB in aqueous suspension. Therefore, the increase of dopant content seems to be helpful for the photo-catalytic activity. According to Fig. 5 and Table 2, the photo-catalytic reactivity of doped $TiO_2$ thin film is higher than that of undoped $TiO_2$, which is consistent with the larger specific surface area of doped $TiO_2$ than undoped $TiO_2$.

The increase in photoactivity may be attributed to the combination of different processes: (1) decrease of the energy gap favoring higher photo excitation efficiency under solar radiation, and giving rise to a larger population of excited species (hole–electron pairs); (2) the small particles size favoring the increase in the surface per volume ratio, the scavenging action of photogenerated electrons by $Sn^{4+}$ or $Nb^{5+}$ ions thus preventing the recombination of electron–hole pairs and increasing the lifetime of charge carriers, so that they can take part in photo-catalytic processes; (3) the doping ions $Sn^{4+}$ or $Nb^{5+}$ can act as electron traps, thus facilitating the electron–hole separation and subsequent transfer of trapped electron to the adsorbed $O_2$ which acts as an electron acceptor on the surface of the $TiO_2$; (4) the dopant contribute to prevent the recombination of electron–hole pairs, increasing the lifetime of charge carriers, so that they can take part in photo-catalytic processes. Higher photo-catalytic behavior of Sn/Nb codoped thin film can be the result of higher specific surface area and a band gap in visual and UV wave lengths ranges. Based on Fig. 5a, under UV irradiation T-1 %Nb has better decomposition ability than T-15 %Sn while T-15 %Sn has better decomposition ability under sun light irradiation. This can be caused by higher sun light absorbance of T-15 %Sn and higher UV light absorbance on T-1 %Nb.

TEM micrographs of T-15 %Sn-1 %Nb thin film are shown in Fig. 6a. Surface was consisted of highly dense and uniform nanocrystalline $TiO_2$, with a porous structure and particle size around 10 nm. This figure also shows formation of crack-free thin film on glazed porcelain substrate.

Figure 6b shows the cross-section image of the prepared coating captured by FE-SEM. As the figure shows, the thickness of thin film is about 200 nm. Thin film structure shows a parallel columnar like structure.

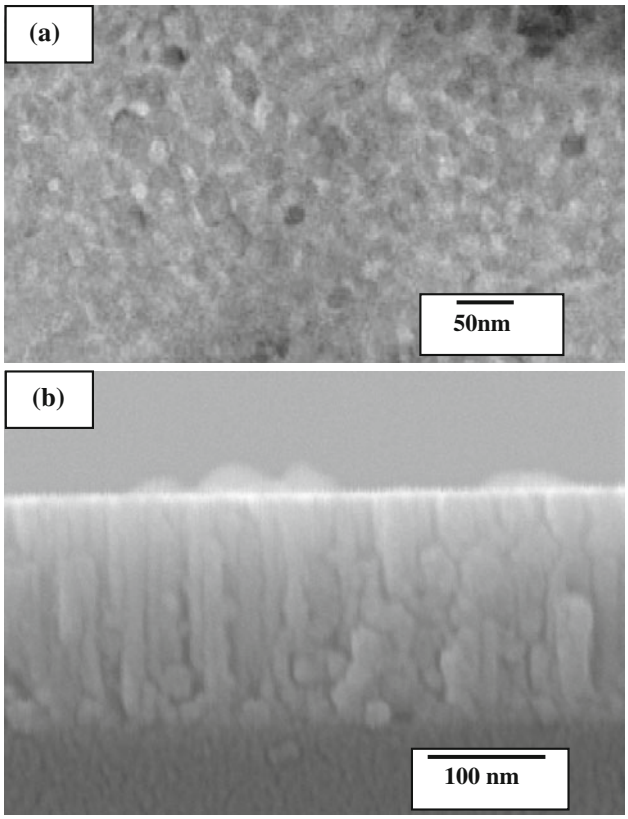


**Fig. 6** **a** TEM image and **b** FE-SEM cross-section image of T-15 %Sn-1 %Nb the thin film calcined at 475 °C for 1 h

TEM images for Sn/Nb co-doped $TiO_2$ thin film is shown in Fig. 7. As seen, both rutile and anatase grains were detected in TEM bright field image. The fringe spacing (*d*) of (101) crystallographic plane is 3.5 Å for undoped $TiO_2$ film [20] and is detected to be 3.55 Å for co-doped $TiO_2$. This implies that $Sn^{4+}$ and $Nb^{5+}$ ions are doped into $TiO_2$ lattice in substitutional space in co-doped $TiO_2$, since the ionic radius of $Sn^{4+}$ (0.71 Å) and the ionic radius of $NB^{5+}$ (0.7 Å) are larger than that of the lattice $Ti^{4+}$ (0.6 Å), a fringe spacing of 3.37 Å corresponding to the (110) planes of rutile $TiO_2$ is observed in co-doped $TiO_2$. All of these are consistent with the aforementioned XRD results.

SAED pattern (Fig. 7-Top right) from a finely dispersed region of Sn/Nb co-doped sample showed continuous rings, which indicate the polycrystalline nature of thin film.

The detailed HR-TEM image analysis of Sn/Nb co-doped $TiO_2$ thin film indicated uniformly substituted Sn and Nb in $TiO_2$ structure. The Sn and Nb ions are incorporated into the structure of titania coatings, which has been confirmed by SAED analysis. No rings corresponding of secondary phases, like $SnO_2$ or $Nb_2O_5$, were observed in SAED pattern for co-doped $TiO_2$ samples.

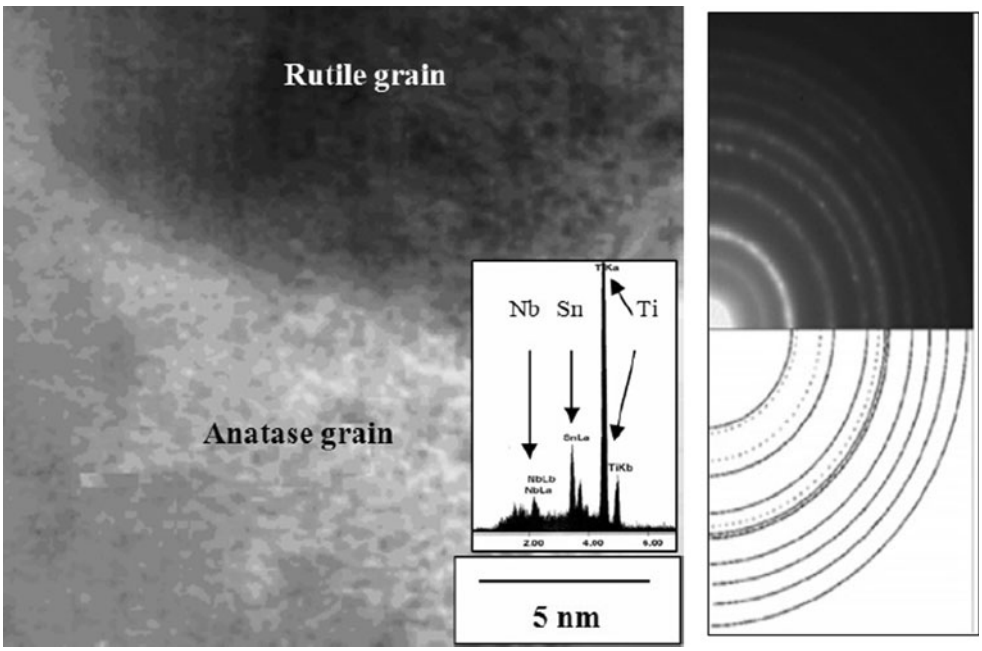


**Fig. 7** Bright field TEM image of Sn/Nb co-doped $TiO_2$ thin film. SAED pattern from this sample is shown in the *right panel* (Anatase $TiO_2$ (*solid lines*) and Rutile $TiO_2$ (*dotted lines*) is shown in the *inset*)

## 4 Conclusion

In this research, Sn/Nb co-doped $TiO_2$ thin films with photo-catalytic properties have been prepared by a sol–gel dip-coating method. The thickness of the applied thin films on porcelain substrates was about 200 nm. The photo-catalytic activity of the co-doped thin film is higher than that of pure $TiO_2$ thin films. $Sn^{4+}$ and $Nb^{5+}$ substitution for $Ti^{4+}$ in the titania lattice results in a decrease in the rate of photogenerated electron–hole recombination that is responsible for the enhancement in photo-catalytic degradation rate. The anatase to rutile phase transformation was promoted by $Sn^{4+}$ doping but inhibited by $Nb^{5+}$ doping. Photo-catalytic activity of the co-doped thin film under solar irradiation was improved comparing to single doped thin films.

## References

1. Yin S, Ihara K, Aita Y, Komatsu M, Sato T (2006) J Photochem Photobiol A Chem 179:105–114
2. Yin S, Yamaki H, Komatsu M, Zhang Q, Wang J, Tang Q (2003) J Mater Chem 13:2996–3001
3. Colon G, Hidalgo MC, Munuera G, Ferino I, Cutrufello MG, Navio JA (2006) Appl Catal B Environ 63:45–59
4. Kato H, Kudo A (2002) J Phys Chem B 106:5029–5034
5. Li FB, Li XZ, Hou MF, Cheah KW, Choy WCH (2005) Appl Catal A General 285:181–189
6. Kubacka A, Fuerte A, Martinez-Arias A, Fernandez-Garcia M (2007) Appl Catal B Environ 74:26–33
7. Jin Z, Zhang X, Li Y, Li S, Lu G (2007) Catal Commun 8:1267–1273
8. Cao Y, He T, Zhao L, Wang E, Yang W, Cao Y (2009) J Phys Chem C 113:18121–18124
9. Xie Y, Yuan C (2004) Appl Surf Sci 221:17–24
10. Bouras P, Slathatos E, Lianos P (2007) Appl Catal B Environ 73:51–59
11. Kudo A (2007) Int J Hydrogen Energy 32:2673–2678
12. Ranjit KT, Willner I, Bossmann SH, Braun AM (2001) J Catal 204:305–313
13. Shifu C, Lei C, Shen G, Gengyu C (2006) Mat Chem Phys 98:116–120
14. Cuiying H, Wansheng Y, Ligin D, Zhibin L, Zhengang S, Lancui Z (2006) Chin J Catal 27:203–209
15. Ihara T, Miyoshi M, Ando M, Sugihara S, Iriyama Y (2001) J Mater Sci 36:4201–4207
16. Ihara T, Miyoshi M, Iriyana Y, Matsumoto O, Sugihara S (2003) Appl Catal B Environ 42:403–409
17. Kuznetsov VN, Serpone N (2006) J Phys Chem B 110:25203–25209
18. Prokes SM, Gole JL, Chen X, Burda C, Carlos WE (2005) Adv Funct Mater 15:161–167
19. Belver C, Bellod R, Stewart SJ, Requejo FG, Fernandez- Garcia M (2006) Appl Catal B Environ 65:309–314
20. Koozegar Kaleji B, Sarraf-Mamoory R, Nakata K, Fujishima A (2011) J Sol-Gel Sci Technol 60:99–107
21. Koozegar Kaleji B, Sarraf-Mamoory R, Nakata K, Fujishima A (2012) Mater Chem Phys 132:210–215
22. Baker RW (2004) Membrane technology and application. Wiley Pub, Chichester
23. Sharma R, Bhatnagar M (1999) Sens Actuators B 56:215–219
24. Fresno F, Coronado JM, Tudela D, Soria J (2005) Appl Catal B Environ 55:159–167
25. Tai WP, Oh JH (2002) Sens Actuators B 85:154–157
26. Kumar KN, Fray DJ, Nair J, Mizukami F, Okubo T (2007) Scripta Mater 57:771–774
27. Klug P, Alexander LE (1974) X-ray diffraction procedures. Wiley, New York
28. Spurr RA, Myers H (1957) Anal Chem 29:760–762
29. Sayilkana F, Asilturka M, Kirazb N (2009) J Hazard Mater 162:1309–1316

30. Sanjines R, Tang H, Berger H, Gozzo F, Margaritondo G (1994) J Appl Phys 75:2945–2951
31. Cao Y, Yang W, Zhang W, Liu G, Yue P (2004) New J Chem 28:218–222
32. Moulder JF, Stickle WF, Sool PE, Bomben KD (1992) Handbook of X-ray photoelectron spectroscopy. Perkin-Elmer, Eden Prairie
33. De Boer JH, Everett BH, Stone FS (1985) Properties of porous materials. Butterworths, London
34. Yang Y, Chen X, Feng Y, Yang G (2007) Nano Lett 7:3879–3883
35. Hu L, Yoko T, Kozuka H, Sakka S (1992) Thin Solid Films 219:18–23
36. Wang Z, Helmersson U, Kall PO (2002) Thin Solid Films 405:50–54
37. Fujishima A, Rao TN, Tryk DA (2000) J Photochem Photobiol C Photochem Rev 1:1–21
38. Kamat PV (1993) Chem Rev 93:267–300